4171 Revision 1

Ulian, Valdrè, Corno, Ugliengo: Ab initio modelling of hydroxyl- and carbonated apatite

* E-mail: giovanni.valdre@unibo.it

Periodic ab initio bulk investigation of hydroxylapatite and type A carbonated apatite with both pseudopotential and all electron basis sets for calcium atoms

Gianfranco Ulian[1], Giovanni Valdrè[1,]*, Marta Corno[2] and Piero Ugliengo[2]

1 Dipartimento di Scienze della Terra e Geologico-Ambientali, Centro di Ricerca Interdisciplinare di Biomineralogia, Cristallografia e Biomateriali, Università di Bologna "Alma Mater Studiorum" Piazza di Porta San Donato 1, 40126 Bologna, Italy

2 Dipartimento di Chimica and NIS Centre of Excellence, University of Torino, Via P. Giuria 7, 10125 Torino, Italy

Abstract

Apatite minerals draw the attention of many researchers not only in mineralogy, but also in biology, biochemistry, and medicine because hydroxylapatite [$Ca_{10}(PO_4)_6(OH)_2$] is the main component of the mineral phase of mammalian bones. However, in nature this mineral is mostly present with various stoichiometric defects. The carbonate ion is found commonly in its structure where it can occupy different crystallographic sites; however, its configurational energy and relative orientation in the apatite lattice is still debated.

In this work, bulk structural features of hexagonal hydroxylapatite (space group $P6_3$) and type A carbonated apatite [$Ca_{10}(PO_4)_6(CO_3)$, space group $P1$] have been modeled by density function method using the hybrid B3LYP functional and an all-electron polarized double-zeta quality Gaussian-type basis set using CRYSTAL09 computer program. The effect on the structural parameters due to improving the Ca pseudopotential, usually adopted in previous studies on hydroxylapatite, towards the present all-electron basis set has also been briefly addressed. Different orientations of the carbonate ion in the apatite unit-cell have been considered. The B3LYP functional and Gaussian-type basis set with polarization have been adopted. The geometry of the model (lattice parameters and internal coordinates) has been fully optimized and resulted in very good agreement with XRD data reported in literature that suggest a "close" configuration (type A1) of the carbonate ion, i.e., with a C-O bond perpendicular to the **c**-axis of the apatite cell.

Keywords: Hydroxylapatite, type A carbonated apatite, periodic ab initio quantum mechanics, DFT

Introduction

Apatite minerals are found in almost all igneous rocks and also in some metamorphic and sedimentary ones. The most important member of the apatite family, both as

naturally occurring mineral and as synthetic compound, is hydroxylapatite OHAp [$Ca_{10}(PO_4)_6(OH)_2$]. As shown by X-ray diffraction (XRD) analysis performed by Suda and co-workers (1995), OHAp can be found in nature as two polymorphs: monoclinic [$P2_1/b$] or hexagonal [$P6_3/m$]. The monoclinic cell is obtained from the hexagonal one by doubling the **b** parameter and presents hydroxyl columns with different OH orientations along the **c**-axis (Rabone and de Leeuw 2005). The hexagonal cell ($a = b$) is related to the monoclinic structure when the glide plane b is a mirror plane m and the twofold axis is a 6_3 axis (Corno et al. 2006). Suda and co-workers (Suda et al. 1995) observed also that at low temperature, the monoclinic cell is more stable than the hexagonal one; the phase transition between the two polymorphs (order/disorder) takes place at 200 °C. The hexagonal OHAp is an extremely important phase, because it is the inorganic component of mammalian bone tissues. OHAp may contain a certain amount of compositional defects, the most abundant is the carbonate ion (CO_3^{2-}, ~6% in weight). The presence of CO_3^{2-} in the mammalian OHAp is necessary to stabilize the hexagonal structure at room temperature (Suda et al. 1995).

Since the first half of the 20th century, researchers were interested in the role of OHAp as a biomaterial for bone and tooth repair, reconstruction and replacement (Albee 1920). However, to improve biocompatibility, the biomaterial should be similar to the bone tissue mineral phase, rather than to pure hydroxylapatite.

The structure of hexagonal OHAp allows extensive atomic substitution and non-stoichiometry in Ca, P, and OH channel sites. For example, anions such as fluoride, chloride and carbonate can easily enter in the channel parallel to the **c**-axis, leading to fluoro-, chloro- and carbonate apatites, both as end-members and in mutual solid solutions (Elliott 1998; Hughes and Rakovan 2002). Many experimental works (Antonakos et al. 2007; Fleet 2009; Fleet and Liu 2003, 2004, 2007; Fleet et al. 2011; Sturgeon and Brown 2009; Suetsugu et al. 1998) and theoretical studies (Astala and Stott 2005; Peroos et al. 2006; Rabone and de Leeuw 2007; Stott and Yin 2003; Zahn and Hochrein 2008) have been done to better understand the role and the positions of CO_3^{2-} in the hydroxylapatite lattice. It appears that the carbonate ion can substitute both OH^- in the **c**-axis channel of apatite (type A) and the phosphate group (type B). This is suggested by Fourier transform infrared (FTIR) analysis showing that the normal modes of the carbonate group fall at different frequencies according to the site occupied by the anion (Fleet and Liu 2003; Fleet and Liu 2004; Fleet and Liu 2007).

Despite many results provided by experimental and theoretical investigations, carbonated hydroxylapatite presents some unclear features and it is still debated. There is not a full agreement on the entity of the crystallographic lattice variations due to the carbonate ion substitutions and on the preferred geometrical orientation of the CO_3^{2-}, especially relative to the calcium channel ion of type A carbonated hydroxylapatite.

The carbonate ion in OHAp may constitute both a negatively and a positively charged defect if it substitutes an OH^- or a PO_4^{3-}, respectively. While for type A the charge compensation usually takes place by OH vacancies, in type B carbonated hydroxylapatite there are many possible ways to restore the neutrality, for example by combinations of hydroxyl group and calcium ion vacancies, which can produce different effects on the geometry of the structure (Astala and Stott 2005). In the present work, we deal with only type A carbonate substitution. The modeling of type B carbonated hydroxylapatite will be the subject of a future work.

There are three proposed CO_3^{2-} configurations in the type A apatite cell (see Fig. 1). Interpretation of experimental FTIR spectra suggested two possible configurations for the CO_3^{2-} in the Ca^{2+} channel. The first one is a "close" configuration (type A1) in which a C-O bond is perpendicular to the **c**-axis (space group *P*$\bar{3}$) (Fleet and Liu 2003; Fleet et al. 2011). This configuration was also investigated by two different theoretical approaches. A static-lattice cluster of a type A carbonated apatite supermolecule (SM) evaluated by Hartree-Fock methods (Peeters et al. 1997) and a periodic lattice calculated using the density functional theory (DFT) with a generalized gradient approximation (GGA) and pseudopotentials on all the atoms of the structure (Astala and Stott 2005).

The second one is an "open" configuration (type A2), where a C-O bond is parallel to the **c**-axis (space group *P*$\bar{6}$) (Suetsugu et al. 1998). Both the close and open configurations have the CO_3^{2-} molecular plane parallel to the apatite (100) crystallographic plane.

The third carbonate configuration (planar) was proposed and investigated by Peroos and co-workers using static and dynamic quantum mechanics (QM) methods adopting empirical interatomic potentials (Peroos et al. 2006). In this configuration, the CO_3^{2-} molecular plane is parallel to the (001) plane and all the C-O bonds are perpendicular to the **c**–axis. However, QM proved that this configuration is not energetically favorable. Also, there is no experimental evidence of this kind of orientation of the carbonate ion (Fleet et al. 2011).

The aim of the present research is to investigate in details type A carbonated apatite (CAp) by periodic ab initio quantum mechanics modeling using both the proposed modeling approach of Corno and co-workers (2006) with pseudopotential on calcium atoms and, for the first time, an all electron basis set for all the atoms of the carbonated apatite structure. The steps of the modeling with the CO_3^{2-} in different configurations were the following: first we simulated an OHAp bulk cell, then we removed the OH^- groups and placed the carbonate ion in one of the equivalent orientation within the selected configuration (open, close and planar). The crystallographic parameters of the optimized structures were compared with the data presented in literature.

Computational details

All calculations have been performed on a Debian (Linux) Cluster with the ab initio CRYSTAL09 code (Dovesi et al. 2009), which implements the Hartree–Fock and Kohn–Sham self consistent field method for the study of periodic systems. All graphical drawings have been carried out with the molecular graphics program MOLDRAW (Ugliengo 2009).

Basis set

Multielectron wave functions are described by linear combination of crystalline orbitals (CO), expanded in terms of Gaussian-type basis sets. The basis sets have been chosen from optimized ones used by other authors for their investigations of OHAp, CAp or similar structures. Calcium has been described with two different basis sets. The first one is a Hay-Wadt Small Core Pseudopotential (HWSCP) (Hay and Wadt, 1985), proposed and modified by Corno and co-workers (2006) for their study on pure hydroxylapatite mineral. The second adopted basis set for calcium atoms is a 8-6511G(2d), used by other authors for calcite (Valenzano et al. 2006), with outer shell exponents $\alpha_{sp} = 0.453$ bohr^{-2}, $\alpha_{d1} = 3.1910$ and 0.8683 bohr^{-2} and $\alpha_{d2} = 0.2891$ bohr^{-2}.

For all the calculations, the phosphorus atom is described by the basis 85-21G(d), α_{sp} = 0.48105 and 0.135 bohr^{-2} and α_d = 0.74583 bohr^{-2}, respectively. Oxygen and hydrogen are both represented by a 6-31G* basis set with the outer shell exponents α_{sp} = 0.2742 bohr^{-2} and α_d = 0.538 bohr^{-2}; and α_{sp} = 0.1613 and α_p = 1.1 bohr^{-2}, respectively. P, O, and H basis sets have been tested and adopted in previous works on hydroxylapatite (Corno et al. 2006). Finally, the carbon atom is described by a 6-21G* basis set with α_{sp} = 0.26 bohr^{-2} and α_d = 0.8 bohr^{-2}, previously adopted for magnesite (Catti et al. 1993).

Hamiltonian and computational parameters

The Becke three-parameter (B3LYP) hybrid exchange functional (Becke 1993) in combination with the gradient-corrected correlation functional of Lee, Yang, and Parr (Lee et al. 1988) has been adopted for all calculations. This functional has been already used for alkali oxides, α-quartz, calcite and hydroxylapatite (Dovesi et al. 1991; Pascale et al. 2004; Prencipe et al. 2004; Corno et al. 2006). The presence of some fraction of exact exchange increases the electronic localization, which in turn increases the ionic nature of the materials, causing a systematic decrease of the lattice parameters and an increase of the elastic constants and bulk moduli. Standard DFT (with local-density approximation and generalized gradient approximation) and Hartree-Fock methods yield systematic errors with opposite signs. The hybrid functionals provide more accurate results (Corà et al. 2004). The exchange–correlation contribution is performed over a grid of points and is the result of a numerical integration of the electron density and its gradient. The adopted pruned grid is given by 75 points and 974 angular points, subdivided into 5 sub-intervals of 86, 194, 350, 974, and 350 points (75, 97-XLGRID) and obtained from the Gauss–Legendre quadrature and Lebedev schemes (Prencipe et al. 2004). This is a good compromise between accuracy and cost of calculation for geometry optimization and vibrational frequencies. The values of the tolerances that control the Coulomb and exchange series are the default provided by CRYSTAL09 (*ITOL*1 to *ITOL*4 = 6) (Dovesi et al. 2009), but we increased the pseudo-overlap parameter (*ITOL*5) from 12 to 14. The Hamiltonian matrix has been diagonalized (Monkhorst and Pack 1976) using a shrinking factor of *IS* = 4 (Dovesi et al. 2009) that leads to 12 and 36 reciprocal lattice points (k-points) for OHAp and CAp, respectively.

Geometry

Lattice constants and internal coordinates have been optimized within the same run using the analytical gradient method for the atomic positions and a numerical gradient for the unit-cell parameters. The Hessian matrix is upgraded with the Broyden–Fletcher–Goldfarb–Shanno algorithm. The tolerances for the maximum allowed gradient and the maximum atomic displacement for considering the geometry as converged have been set to 0.00006 hartree bohr^{-1} and 0.00012 bohr, respectively.

Vibrational features

Within the harmonic approximation and in periodic systems, the phonon frequencies at Γ point are evaluated by diagonalising the central zone (k = 0) mass-weighted Hessian matrix

$$W_{ij}(k=0) = \sum_{G} \frac{H_{ij}^{0G}}{\sqrt{M_i M_j}}$$

where H^{0G}_{ij} is the second derivative of the electronic + nuclear repulsion energy E evaluated at equilibrium **u = 0**. The Hessian at equilibrium was obtained by numerical differentiation of the analytical first derivative, calculated at geometries obtained by small increments, υ, in each of the 3N nuclear coordinates with respect to the equilibrium geometry. An extensive discussion of the computational conditions and other numerical aspects concerning the calculation of the vibrational frequencies at Γ point can be found in the literature (Pascale et al. 2004; Tosoni et al. 2005).

The use of the B3LYP hybrid functional and all-electron basis set provides a good accuracy to the quantum mechanics simulations of solid phases with respect to the experimental results. However this improvement is expensive in terms of computational resources. In particular, we compared the optimization of the OHAp structure using both a pseudopotential (Habas et al. 1998) and the all-electron basis set on the calcium ions. While the different methods did not affect the number of optimization steps, the time needed to reach convergence is increased roughly by a factor of 2 when all-electron basis sets are used. This imposes a severe limit when larger cell are required or when the number of heavy atoms increases. It will be shown in the next sections that the differences of the equilibrium geometries obtained by the different methods are about 2% on lattice parameters, as observed in the comparison with the result of Astala and Stott (2005) and Corno and co-workers (2006). However, it was observed in an earlier work by Valenzano et al. (2006) that the effect of the use of different basis sets and geometries are important for vibrational calculations. Richer basis sets are required to obtain more accurate data.

Results and discussion

Quantum mechanics modeling of hydroxylapatite (OHAp)

Corno and co-workers (2006) have recently modeled the hydroxylapatite structure by ab initio quantum mechanics methods adopting an all electron basis set, except for the pseudopotentials for the calcium ions. The simulations referred to a structure of OHAp experimentally derived by XRD (Hughes et al. 1989). The unit-cell contains 44 atoms and two unit formula (Z = 2) of $Ca_5(PO_4)_3(OH)$. To take into account the half occupancy of the oxygen and hydrogen atoms of the hydroxyl group, Hughes and co-workers (1989) assigned a mirror plane *m* to the refined structure ($P6_3/m$ space group). However, Corno and co-workers (2006) noted that within the experimentally observed $P6_3/m$ space group one cannot simulate the hexagonal OHAp because of the non-physical duplication of each OH group by the mirror plane. To avoid this situation, they reduced the symmetry to a $P6_3$ space group, in which all the OH groups maintain the same alignment in each column within the OHAp structure (see Fig. 2). As a consequence of the symmetry reduction, the number of non-equivalent calcium atoms increases from two to three (Ca1, Ca2, and Ca3). The Ca1 atom has three O atoms as neighbors, Ca2 has six and Ca3 has four. The two hydroxyl groups are oriented in the same direction, along the **c** axis. Each hydroxyl group is placed in the center of an equilateral triangle described by three Ca3 atoms. The results provided by their simulations were in agreement with the experimental

results of Hughes and co-workers (1989) and of Saenger and Kuhs (1992) (see Table 1 for a comparison).

In the present work, we simulated the OHAp structure following the model of Corno and co-workers (2006), but we adopted a complete basis set for all atoms in the structure and the pseudopotential approximation on the Ca ion was completely removed. The optimization results are reported in Table 1 and graphically shown in Figure 2. In Table 1, the results were compared to those of the structure modeled by Corno et al. (2006) and to those experimentally obtained by single-crystal XRD (Hughes et al. 1989) and neutron diffraction (Saenger and Kuhs 1992). The structural features obtained from our simulation are slightly different with respect to those of Corno et al. (2006) because of the more complete basis set adopted. The cell parameters that we have obtained ($a = b =$ 9.433 Å, c = 6.896 Å) are very close to the experimental ones from XRD (Δa = +0.016 Å, Δc = +0.021 Å) and neutron diffraction (Δa = +0.008 Å, Δc = +0.012 Å). The mean bond lengths of P-O and Ca3-O interaction distances in our models are 1.551 Å and 2.391 Å, respectively. These results match very well with the ones from experimental analysis, with only a slight overestimation of the P-O bond lengths (Δ_{XRD} = +0.019 Å, $\Delta_{Neutron}$ = +0.015 Å) and a minimal underestimation of the Ca3-O interactions (Δ_{XRD} = –0.007 Å, $\Delta_{Neutron}$ = –0.009 Å). In particular, there is a very good agreement with the specific P-O and Ca-O bond/interaction lengths measured by Hughes et al. (1989), confirming the good choice of computational parameters, especially the rich basis set. All the atomic positions of the modeled OHAp can be found in the crystallographic information framework (CIF[1]) data file.

Quantum mechanics modeling of type A carbonated apatite (CAp)

The substitution of an OH ion by a CO_3 as in type-A carbonated apatite (independently of the sub type A1, A2, or planar) requires charge compensation. The simplest way to achieve this is the removal of the hydroxyl group remaining in the cell leading to the CAp cell with unit formula $Ca_{10}(PO_4)_6(CO_3)$. This method has also been adopted by Astala and Stott (2005) and by Peroos et al. (2006).

QM modeling involved initially the three configurations (A1, A2, and planar) described in the introduction and reported in Figure 1. In Table 2, all the details of the lattice parameters and bond lengths/angles for the three models optimized both the all-electron and pseudopotential on the Ca atom have been reported. In Table 3 the most stable carbonated apatite structures have been compared with the measured XRD data of Fleet and Liu (2003).

Type A1 configuration

The simulation was performed in absence of symmetry (space group *P*1) with two main advantages: no undesired atom is generated and the geometry optimization is unconstrained. This condition also allowed the carbonate ion to rotate and/or displace itself, passing through all the intermediate orientations until the minimum of energy was found.

The carbonate ion was placed with the central atom C at (x/*a*, y/*b*, z/*c*) = (0.0, 0.0, 0.5), in an intermediate position with respect to the two originally present hydroxyl ions that have been substituted by the CO_3^{2-} group in the OHAp cell. C-O bond lengths and OCO bond angles were set to 1.25Å and 120°, respectively.

The results from the geometry optimization of the models showed that the type A1 configuration was energetically favored with both the adopted basis sets, with a C-O bond (bisector of the CO_3^{2-} plane) perpendicular to the **c**-axis and the plane of the molecule slightly canted within the (100) plane by about 6° (Figs. 3a and 3b).

Each oxygen of the carbonate ion interacts electrostatically with two Ca^{2+} of the apatite structure (Figs. 3c and 3d) with a mean interaction distance of 2.39 Å. The local geometry of CO_3^{2-} is very close to that of calcite, where the same O_{CO3} — Ca^{2+} interaction at 2.34 Å has been observed (Maslen et al. 1993).

Our simulation of CAp showed also that the two calcium ions in the channel placed on the (100) plane are shifted along the [010] direction with their relative distance increased from 5.84 Å (in OHAp) to 6.42 Å (in CAp). For the two Ca^{2+} along [100], their distance is slightly increased (+0.22 Å). The other remaining two calcium ions in the channel have not been significantly displaced (<0.001 Å) with respect to their position in OHAp. This general distortion from the ideal hexagonal channel allows the accommodation of the carbonate ion in the apatite structure.

The phosphate ions are slightly displaced to maintain a constant P-Ca^{2+} mean distance of 3.67 Å. The same value has been observed for pure OHAp. The internal bond lengths and angles of the PO_4^{3-} tetrahedrons are slightly modified from the ideal ones to minimize the sterical encumbrance and optimize the electrostatic interaction with the surrounding ions. All the atomic positions of the modeled CAp can be found in the crystallographic information framework (CIF) data file.

In type A1 configuration, the main effect of the $CO_3^{2-}/2OH^-$ substitution is the increase of *a* and *b* cell parameters (*a* = 9.582 Å, *b* = 9.764) and a contraction of *c* (*c* = 6.877 Å). Despite the lack of symmetry, the unit-cell angles (α, β, γ) show only slight differences from the pure hydroxylapatite ones. Our structural observations are in good agreement with the results of the earlier theoretical works of Peeters et al. (1997) and Astala and Stott (2005). We observed an opposite effect on the *a*, *b*, α, and γ lattice parameters compared to those of type-A ordered CAp by Astala and Stott (2005), because of the different orientation of the carbonate ion in the unit cells.

Because the experimentally refined structures available in literature are not of pure carbonated apatite, the comparison of our model was made with the structure of the more carbonate-rich carbonated apatite (0.75CAp·0.25OHAp) that was characterized by single-crystal XRD and FTIR by Fleet and Liu (2003) and Fleet et al. (2011). The crystallographic parameters, bond lengths and angles of type A1 configuration modeled in our work are in very good agreement with those experimentally refined (see Table 2). The slight difference on the *b* lattice parameter may arise because the absence of symmetry constrains in the modeled CAp allowed a relaxation of the structure primarily along the **b**-axis. The carbonate ion plane is parallel to this direction and causes a stretch in the Ca^{2+} channel to minimize sterical encumbrance. Also, worth to be noted that our model refers to a pure carbonated apatite (CAp).

The results of our modeling are in agreement also with FTIR analysis. In Figure 4, we reported a comparison between the simulated vibrational spectra obtained by our model and those experimentally observed by Fleet and Liu (2003). In the figure, the asymmetrical stretching and the out-of-plane bending of the type A1 carbonate ion have been labeled as ν_3 and ν_2, respectively. ν_3 consists in a doublet in the 1600-1500 cm^{-1} region, with peaks centered at 1604 and 1518 cm^{-1}. These signals slightly shifted at

higher wavenumbers than those observed by Fleet and Liu (2003) and Fleet et al. (2011). However, the separation between the two peaks obtained by the simulation is very close to the experimental one, 86 and 83 cm^{-1}, respectively. For the out-of-plane (ν_2) vibrational mode, we obtained a band centered at 878 cm^{-1}, the same value observed by Fleet and Liu (2003) and Fleet et al. (2011).

Type A2 configuration

The unconstrained geometrical optimization of the CAp structure starting with the CO_3^{2-} in type A2 configuration brought the carbonate ion toward type A1 configuration through a molecular rotation of the CO_3^{2-} (see in Fig. 1 the difference between the close and open configurations). This effect was also obtained adopting the pseudopotential on Ca atoms. The observed angle of rotation (30°) was the minimum angular value needed to pass from the open to the close configuration. The A2/A1 transition is in agreement with the results of Fleet et al. (2011), where they observed that type A1 is the preferred configuration.

Planar configuration

The planar configuration model was created with the CO_3^{2-} molecular plane parallel to the (001) cell plane. It was geometrically optimized with *P*3 and *P*1 space group symmetry. We observed two different results when adopting the proposed basis sets. Using the pseudopotential on calcium atoms, the carbonate ion was displaced and brought in the A1 configuration removing the symmetry constrains. Instead, with the all electron basis the planar configuration was maintained both with and without symmetry, although the difference in the crystal intrinsic electronic energy is very high if compared with the close configuration, resulting +165.78 kJ/mol for the *P*3 structure and +164.78 kJ/mol for the unconstrained one (*P*1). To better understand the nature of this difference, we calculated the vibrational features and we found that the planar configuration represents a saddle point on the potential energy surface. However the details of this investigation are beyond the scope of the present paper and will be the subject of a forthcoming work dedicated to the vibrational properties of carbonated apatite.

References cited

Albee, F.H. (1920) Studies in bone growth—Triple calcium phosphate as stimulus to osteogenesis. Annals of Surgery, 71, 32–39.

Antonakos, A., Liarokapis, E., and Leventouri, T. (2007) Micro-Raman and FTIR studies of synthetic and natural apatites. Biomaterials, 28, 3043–3054.

Astala, R. and Stott, M.J. (2005) First principles investigation of mineral component of bone: CO_3 substitutions in hydroxyapatite. Chemistry of Materials, 17, 4125–4133.

Becke, A.D. (1993) Density-Functional Thermochemistry. 3. The Role of Exact Exchange. Journal of Chemical Physics, 98, 5648–5652.

Catti, M., Pavese, A., Dovesi, R., and Saunders, V.R. (1993) Static lattice and electron properties of $MgCO^3$ (Magnesite) calculated by ab-initio periodic Hartree-Fock methods. Physical Review B, 47, 9189–9198.

Corà, F., Alfredsson, M., Middlemiss, D.S., Mackrodt, W.C., Dovesi, R., and Orlando, R. (2004) The performance of hybrid density functionals in solid state chemistry. In J. McGrady and N. Kaltsoyannis, Eds., Density Functional Theory in Inorganic Chemistry, p. 171–232. Springer-Verlag, Heidelberg.

Corno, M., Busco, C., Civalleri, B., and Ugliengo, P. (2006) Periodic ab initio study of structural and vibrational features of hexagonal hydroxyapatite $Ca_{10}(PO_4)_6(OH)_2$. Physical Chemistry Chemical Physics, 8, 2464–2472.

Dovesi, R., Roetti, C., Freyria Fava, C., Prencipe, M., and Saunders, V.R. (1991) On the elastic properties of lithium, sodium an potassium oxide. An ab initio study. Chemical Physics, 156, 11–19.

Dovesi, R., Saunders, V.R., Roetti, C., Orlando, R., Zicovich-Wilson, C.M., Pascale, F., Civalleri, B., Doll, K., Harrison, N.M., Bush, I.J., D'Arco, P., and Llunell, M. (2009) CRYSTAL09, User's Manual. Università di Torino, Torino, Italy.

Elliott, J.C. (1998) Recent studies of apatites and other calcium orthophosphates. In E. Bre`s, and P. Hardouin, Eds., Les mate'riaux en phosphate de calcium. Aspects fondamentaux, 25–66. Sauramps Medical, Montpellier.

Fleet, M.E. (2009) Infrared spectra of carbonate apatites: n2-Region bands. Biomaterials, 30, 1473–1481.

Fleet, M.E. and Liu, X. (2003) Carbonate apatite type A synthesized at high pressure: new space group (*P*3̄) and orientation of channel carbonate ion. Journal of Solid State Chemistry, 174, 412–417.

——— (2004) Location of type B carbonate ion in type A-B carbonate apatite synthesized at high pressure. Journal of Solid State Chemistry, 177, 3174–3182.

——— (2007) Coupled substitution of type A and B carbonate in sodium-bearing apatite. Biomaterials, 28, 916–926.

Fleet, M.E., Liu, X.Y., and Liu, X. (2011) Orientation of channel carbonate ions in apatite: Effect of pressure and composition. American Mineralogist, 96, 1148–1157.

Habas, M.P., Dovesi, R., and Lichanot, A. (1998) The B1 reversible arrow B2 phase transition in alkaline-earth oxides: A comparison of ab initio Hartree-Fock and density functional calculations. Journal of Physics-Condensed Matter, 10, 6897–6909.

Hay PJ, Wadt WR (1985): Ab Initio effective core potentials for molecular calculations. Potentials for main group elements Na to Bi. J. Chem. Phys. 82:284-298.

Hughes, J.M. and Rakovan, J. (2002) The crystal structure of apatite, $Ca_5(PO_4)_3(F,OH,Cl)$. In M.J. Kohn, J. Rakovan, and J.M. Hughes, Eds. Phosphates, 48, 1–12. Reviews in Mineralogy, Mineralogical Society of America, Chantilly, Virginia.

Hughes, J.M., Cameron, M., and Crowley, K.D. (1989) Structural variations in natural F, OH and Cl apatites. American Mineralogist, 74, 870–876.

Lee, C.T., Yang, W.T., and Parr, R.G. (1988) Development of the Colle-Salvetti Correlation-Energy Formula into a Functional of the Electron-Density. Physical Review B, 37, 785–789.

Maslen, E.N., Streltsov, V.A., and Streltsova, N.R. (1993) X-ray study of the electron-density in calcite, $CaCO_3$. Acta Crystallographica Section B-Structural Science, 49, 636–641.

Monkhorst, H.J. and Pack, J.D. (1976) Special points for Brillouin-zone integrations. Physical Review B, 8, 5188–5192.

Pascale, F., Zicovich-Wilson, C.M., Gejo, F.L., Civalleri, B., Orlando, R., and Dovesi, R. (2004) The calculation of the vibrational frequencies of crystalline compounds and its implementation in the CRYSTAL code. Journal of Computational Chemistry, 25, 888–897.

Peeters, A., DeMaeyer, E.A.P., VanAlsenoy, C., and Verbeeck, R.M.H. (1997) Solids modeled by ab initio crystal-field methods. 12. Structure, orientation, and position of A-type carbonate in a hydroxyapatite lattice. Journal of Physical Chemistry B, 101, 3995–3998.

Peroos, S., Du, Z., and de Leeuw, N.H. (2006) A computer modelling study of the uptake, structure and distribution of carbonate defects in hydroxy-apatite. Biomaterials, 27, 2150–2161.

Prencipe, M., Pascale, F., Zicovich-Wilson, C.M., Saunders, V.R., Orlando, R., and Dovesi, R. (2004) The vibrational spectrum of calcite (CaCO3): An ab initio quantum-mechanical calculation. Physics and Chemistry of Minerals, 31, 559–564.

Rabone, J.A.L. and de Leeuw, N.H. (2005) Interatomic potential models for natural apatite crystals: Incorporating strontium and the lanthanides. Journal Computational Chemistry, 27:253–266.

——— (2007) Potential routes to carbon inclusion in apatite materials: a DFT study. Physics and Chemistry of Minerals, 34, 495–506.

Saenger, A.T. and Kuhs, W.F. (1992) Structural disorder in hydroxyapatite. Zeitschrift für Kristallographie, 199, 123–148.

Stott, M.J. and Yin, X. (2003) α- and β-tricalcium phosphate: A density functional study. Physical Review B, 68, 1–8.

Sturgeon, J.L. and Brown, P.W. (2009) Effects of carbonate on hydroxyapatite formed from $CaHPO_4$ and $Ca_4(PO_4)_2O$. Journal of Materials Science-Materials in Medicine, 20, 1787–1794.

Suda, H., Yashima, M., Kakihana, M., and Yoshimura, M. (1995) Monoclinic ↔ Hexagonal phase transition in hydroxyapatite studied by X-ray powder diffraction and differential scanning calorimeter techniques. Journal of Physical Chemistry, 99, 6752–6754.

Suetsugu, Y., Shimoya, I., and Tanaka, J. (1998) Configuration of carbonate ions in apatite structure determined by polarized infrared spectroscopy. Journal of the American Ceramic Society, 81, 746–748.

Tosoni, S., Pascale, F., Ugliengo, P., Orlando, R., Saunders, V.R., and Dovesi, R. (2005) Quantum mechanical calculation of the OH vibrational frequency in crystalline solids. Molecular Physics, 103, 2549–2558.

Ugliengo, P. (2009) MOLDRAW: A molecular graphics program to display and manipulate molecular structures, H1 (32-bit).

Valenzano, L., Torres, F.J., Klaus, D., Pascale, F., Zicovich-Wilson, C.M., and Dovesi, R. (2006) Ab initio study of the vibrational spectrum and related properties of crystalline compounds; the case of $CaCO_3$ calcite. Zeitschrift Fur Physikalische Chemie, 220, 893–912.

Zahn, D. and Hochrein, O. (2008) On the composition and atomic arrangement of calcium-deficient hydroxyapatite: An ab-initio analysis. Journal of Solid State Chemistry, 181, 1712–1716.

FIGURE 1. Views along [001] (left) and [100] (right) of type A CAp with three different configurations of CO_3^{2-}. (A1) "close" configuration, (A2) "open" configuration and "planar" configuration.

FIGURE 2. Optimization results and different views for the bulk structure of hydroxylapatite OHAp. Symmetrically different calcium ions are indicated.

FIGURE 3. Simulation of CAp with carbonate ion in close configuration (type A1). The most stable structure was obtained from full geometry optimization. (**a**) [001] and (**b**) [100] projections. In **c** and **d**, the interactions between CO_3^{2-} and the channel calcium ions are showed along [001] and [100], respectively. Phosphorous, oxygen, and calcium radii were reduced for sake of clearness in **c** and **d**.

FIGURE 4. IR regions relative to type A1 CO_3^{2-} asymmetric stretching ν_3 and out-of-plane bending ν_2. Continuous line refers to our simulated data, whereas dashed line was extrapolated from the results of Fleet and Liu (2003).

[1] Deposit item AM-12-066, CIFs. Deposit items are available two ways: For a paper copy contact the Business Office of the Mineralogical Society of America (see inside front cover of recent issue) for price information. For an electronic copy visit the MSA web site at http://www.minsocam.org, go to the *American Mineralogist* Contents, find the table of contents for the specific volume/issue wanted, and then click on the deposit link there.

TABLE 1. Simulated and experimental results of hydroxylapatite OHAp

	B3LYP*	B3LYP†	XRD‡	Neutron§	Δ_{XRD}	$\Delta_{Neutron}$
Symmetry	$P6_3$	$P6_3$	$P6_3/m$	$P6_3/m$		
a (Å)	9.433	9.329	9.417	9.425	+0.016	+0.008
c (Å)	6.896	6.949	6.875	6.884	+0.021	+0.012
V (Å^3)	532	529	528	530	+4	+2
Bond length (Å)						
P-O1	1.547		1.529		+0.018	
P-O2	1.558		1.537		+0.021	
P-O3	1.551		1.537		+0.014	
P-O4	1.549		1.534		+0.015	
Mean	1.551	1.547	1.532	1.536	+0.019	+0.015
Ca3-Ca3	4.085		4.084		+0.001	
Ca3-O1	2.700		2.711		–0.011	
Ca3-O2	2.350		2.353		–0.003	
Ca3-O3	2.341		2.343		–0.002	
Ca3-O4	2.501		2.509		–0.008	
Ca3-O(H)	2.372		2.385		–0.013	
Mean Ca3-O	2.391	2.41	2.398	2.40	–0.007	–0.009
O-H	0.97	0.97	1.09	0.90	–0.12	+0.07

Notes: Mean Ca3-O distances have been evaluated with values <2.51 Å. Experimental data are referred to single-crystal analysis.
* Present work.
† Corno et al. (2006).
‡ Hughes et al. (1989).
§ Saenger and Kuhs (1992).

TABLE 2. Simulated results of type A CAp with all electron and pseudopotential basis sets on Ca atom

	Ca - All electron				Ca - Pseudopotential			
	A1	A2	Planar		A1	A2	Planar	
Symmetry	*P*1	*P*1	*P*1	*P*3	*P*1	*P*1	*P*1	*P*3
a (Å)	9.582	9.624	9.651	9.654	9.510	9.515	9.327	9.573
b (Å)	9.764	9.708	9.651	9.654	9.572	9.571	9.463	9.573
c (Å)	6.877	6.883	6.832	6.827	6.930	6.928	6.921	6.863
α (°)	89.3	89.5	90	90.0	89.5	89.5	90.2	90.0
β (°)	89.8	89.5	90	90.0	89.2	89.2	89.0	90.0
γ (°)	121.9	121.9	120	120.0	121.4	121.4	118.3	120.0
V_{cc} (Å^3)	546	546	551	551	538.1	538.3	537.6	544.7

Density (g/cm^3)	3.131	3.130	3.102	3.102	3.176	3.175	3.179	3.138
Mean bond length (Å)								
P-O	1.54	1.56	1.56	1.56	1.55	1.51	1.55	1.55
C-O	1.29	1.29	1.28	1.28	1.28	1.29	1.28	1.28
Ca-O_{CO3}	2.39	2.36	2.42	2.42	2.35	2.60	2.33	2.54
Mean bond angle (°)								
O-P-O	110.1	108.8	110.5	110.5	108.8	107.5	108.7	108.9
O-C-O	120.0	120.0	120.0	120.0	120.0	120.0	120.00	120.0

TABLE 3. Differences between experimental (XRD) and simulated results of type A CAp

	XRD*	A1-ae	A1-pp	SM-HF†	GGA-PBE‡
Symmetry	*P*3̄	*P*1	*P*1	–	*P*1
a (Å)	9.521	+0.061	+0.011	9.544	9.88
b (Å)	9.521	+0.243	+0.051	9.544	9.69
c (Å)	6.873	+0.004	+0.057	6.859	7.14
α (°)	90	–0.7	-0.5	90.0	90.9
β (°)	90	–0.2	-0.8	90.0	89.6
γ (°)	120	+0.9	+1.4	120.0	118.7
Density (g/cm^3)	3.152	–0.021	+0.024	–	–
Mean bond length (Å)					
P-O	1.53	+0.01	+0.02	–	–
C-O	1.24	+0.05	+0.04	+0.03	+0.05
Ca-O_{CO3}	2.34	+0.05	+0.01	–	–
Mean bond angle (°)					
O-P-O	109.5	+0.6	-0.7	–	–
O-C-O	120.0	+0.0	+0.0	+0.0	+0.0

Notes: XRD data are referred to single-crystal analysis. A1-ae and A1-pp refers to the present results obtained with all electron and pseudopotential basis sets on Ca atoms, respectively. SM-HF and GGA-PBE results are related to earlier simulations conducted by static lattice/Hartree-Fock and periodic/DFT functionals, respectively. SM-HF lattice parameters have not been optimized.

* Fleet and Liu (2003).

† Peeters et al. (1997).

‡ Astala and Stott (2005).

A1

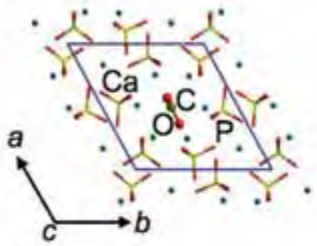

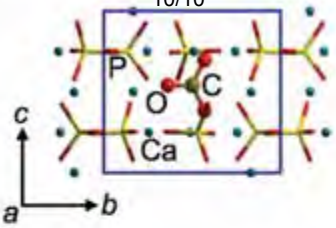

A2

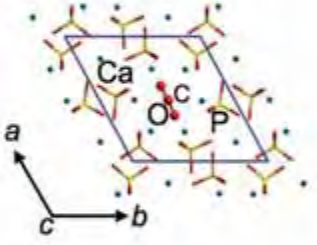

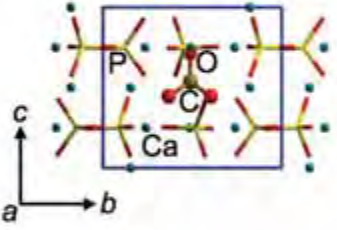

Planar

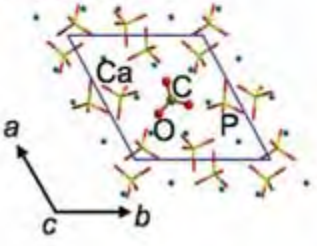

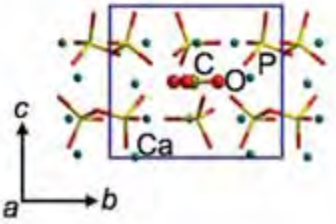

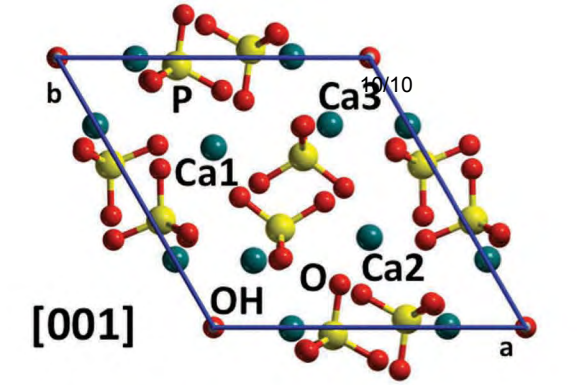
b
P
Ca3
Ca1
O
Ca2
OH
[001]
a

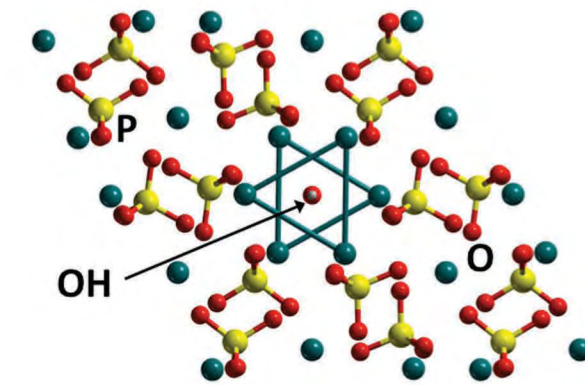
P
OH
O

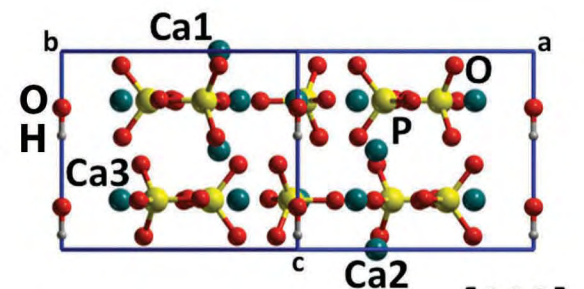
b
Ca1
a
O
H
P
Ca3
c
Ca2
[110]

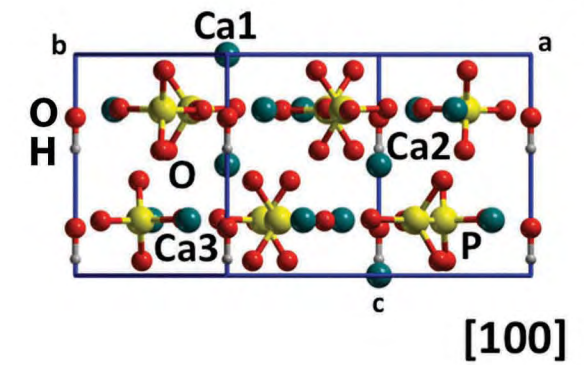
b
Ca1
a
O
H
Ca2
O
Ca3
P
c
[100]

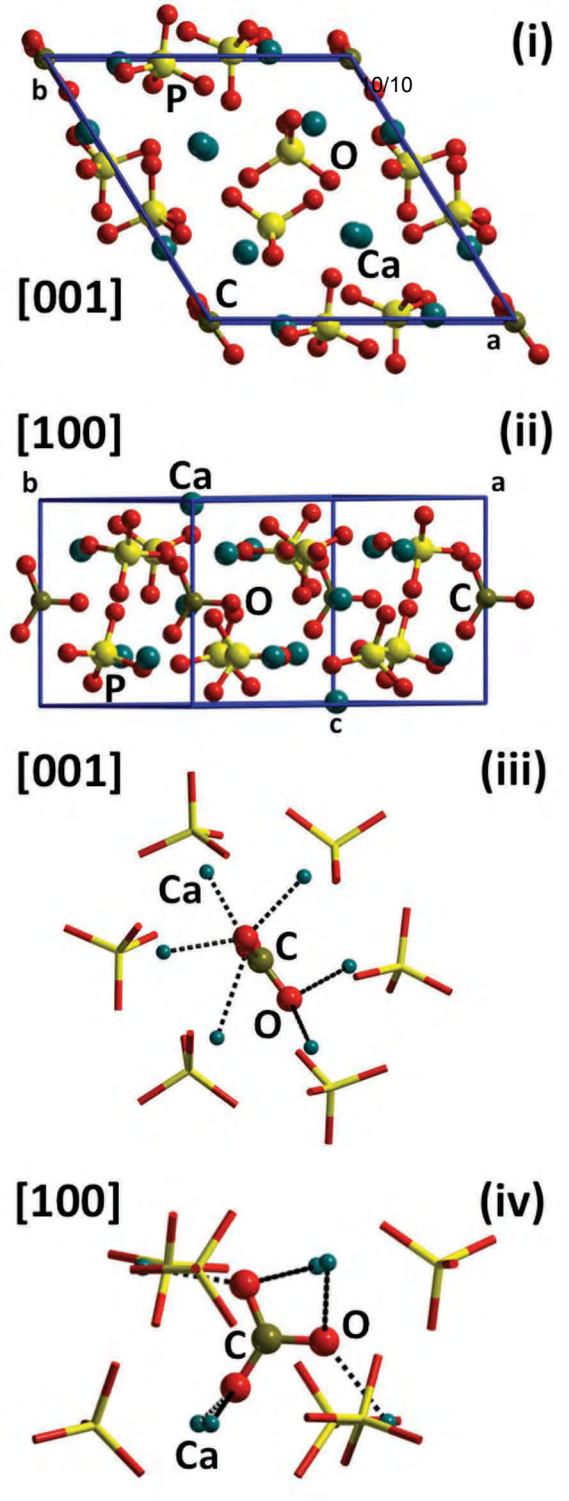
(i)
b
P
O
Ca
[001]
C
a
[100]
(ii)
b
Ca
a
O
C
P
c
[001]
(iii)
Ca
C
O
[100]
(iv)
C
O
Ca

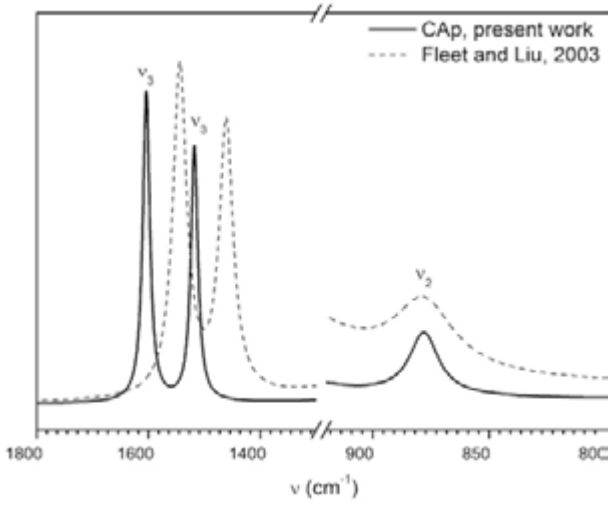
CAp, present work
Fleet and Liu, 2003
ν3
ν1
ν2
1800
1600
1400
900
850
800
ν (cm-1)